PROPERTIES OF (p, n) REACTIONS IN TENUOUS GASES

by

Paul Blair Parks III

Department of Physics
Duke University

A dissertation submitted in partial fulfillment of
the requirements for the degree of Doctor
of Philosophy in the Department of
Physics in the Graduate School
of Arts and Sciences of
Duke University

1963

ABSTRACT

PROPERTIES OF (p, n) REACTIONS IN TENUOUS GASES

by

Paul Blair Parks III

A cryogenic target chamber has been developed for the production of very thin, but uniform, targets to be used with accelerated charged particle beams. The target reaction chamber is appended to a cryostat which is capable of containing liquid helium as the primary refrigerant. The temperature of this chamber can be adjusted so that condensation of the gas in the vicinity of the beam path is eliminated. The cryostat freezes out the gas which escapes the reaction chamber. To date, we have used this new cryogenic technique to study the (p, n) reactions of B^{11}, A^{40}, and Cl^{37}, and also the D(d, n) reaction. Very narrow resonances (widths ≤ 450 ev) are discovered in the $A^{40}(p, n)K^{40}$ reaction near the neutron threshold. We find that the narrower resonances show decided asymmetries which seem independent of target density over the range investigated. The importance of the larger energy losses in ionizing K and L shell electrons is stressed. The majority of these large losses are thought to possibly occur in the atom containing the nucleus with which the proton reacts. The narrowest resonances have apparent widths at half maximum

of 140 ev. This leads to an upper limit on the incident beam spread of about 125 ev. The target thickness appears to be about 100 ev. Use of the T(p, n) reaction as a neutron source is proposed and estimates of the resolving power attainable with this reaction in the cryogenic system are reported.

ACKNOWLEDGEMENTS

This project would not have been possible without the concerted efforts of all the members of the Nuclear Structure Laboratory who aided in testing the cryogenic target. I wish to express sincere thanks to John Farrell, Tom Grissom, and Charles Kyker. Especially do I wish to thank my co-worker Pat Beard for his unselfish close cooperation during the last three years. Under the direct supervision of Dr. E. G. Bilpuch, the system was finally successfully tested and for his intense and exceedingly helpful efforts I express wholehearted appreciation. However, it is to Dr. H. W. Newson that I must voice the most heartfelt thanks, for without his unique leadership contributions and confidence this project would certainly never have come to fruition.

This project was aided immeasurably by many enlightening discussions with Dr. H. W. Lewis, Dr. R. M. Williamson, and most especially Dr. Horst Meier in the matter of cryogenic techniques.

Sincere appreciation is here expressed to Mr. Milton Whitfield and the entire staff of the Duke University Instrument Shop. I must particularly acclaim the exacting craftsmanship of Mr. Alton Lovette who fabricated and assembled most of the components of the cryogenic system; his suggestions were extremely helpful and many of the features of the target chamber originated with him.

We also acknowledge the aid of Miss Dottie Brand in the reduction of the data. Mr. William Meier has, as usual, done yeoman service in the preparation of the figures which appear in this draft. For their expert technical assistance I am also greatly indebted to Mr. Sidney Edwards and Mr. O. C. Duncan.

It is to my wife Patsy, whose gentle encouragement supported me during these graduate days, that I owe the greatest debt. A quiet courage and unquestioning loyalty combine in her to provide for me an inspiring example of integrity and perseverance.

This work was supported in part by the Atomic Energy Commission.

P.B.P.

CONTENTS

LIST OF FIGURES

LIST OF TABLES

PROPERTIES OF (p, n) REACTIONS IN TENUOUS GASES

CHAPTER I

INTRODUCTION

High resolution neutron transmission measurements have enjoyed wide use as a means of studying nuclear resonance phenomena. Cross sections are large since no Coulomb barrier inhibits the formation of compound systems. While interpretation may be relatively easy, the experimental obstacles can be quite serious. The most successful techniques, thus far developed, for producing effectively monoenergetic neutron beams, have fallen into two categories. The difference in these approaches essentially depends on whether the available neutrons are heterogeneous and need to be separated by velocity selection or whether the conditions of the source are carefully controlled so as to produce monoenergetic neutrons in the first place.

In the second category we take advantage of the kinematics of a nuclear reaction which will produce monoenergetic neutrons under the following ideal conditions: (1) Neutron emission to the ground state of the residual nucleus is the only neutron decay energetically allowed. (2) The bombarding particle energy is above back threshold. (3) The

neutrons are all emitted at the same angle θ with respect to the accelerated beam. (4) The incident particles are monoenergetic. (5) The target nuclei are at rest. (6) The target is infinitely thin, i.e., there is no energy loss in the target. The first three conditions are satisfied either by careful selection of the reaction and the experimental conditions or by sacrificing intensity to resolving power. Unfortunately, Van de Graaff accelerators do not produce perfectly monoenergetic beams but an electronic system for minimizing this spread was designed and reported prior to this work (Parks, Newson, and Williamson, 1958), so that condition (4) is very nearly met. The last two conditions are more difficult. The energy loss in a solid target cannot in general be controlled by reducing the amount of target material. Furthermore, the target nucleus is not truly at rest; thus a Doppler distribution exists for the incoming proton since the random motion of the target nucleus creates a spread in the relative velocities in the center of mass system. In essence, our problem has been reduced to one in atomic physics, i.e., to finding a solution for these last two difficulties.

The most commonly used source of nearly monoenergetic neutrons in the kilovolt region is the Li^7 (p, n)Be^7 reaction (Newson, et al., 1957). The limit to the resolution available with this reaction is set by our inability to produce lithium metal targets which are at the same time both thin and uniform. Recent studies on the evaporation of thin films onto suitable backing material, usually tantalum, indicated that there is a lower limit for the effective thickness of lithium targets (Bowman, Bilpuch and Newson, 1962). The average thickness, as indicated by neutron

emission, is usually considerably less than the average energy loss (750 ev minimum). It is surmised that this limit is a result of the process of crystalline growth, i.e., the detailed structure of the target surface is one of hills and valleys.

Since lithium did not seem promising for further improvements in resolution, other possible reactions were investigated. In order to avoid the nonuniformity associated with evaporated films, it was decided to try to develop a gaseous target. $T^3(p, n)He^3$ has kinematic properties that would allow very good resolution for neutrons selected by our 160° neutron collimator (Nichols, Bilpuch, and Newson, 1959). Thus the emphasis at the beginning of this problem was placed on developing a system capable of handling this radioactive isotope of hydrogen.

Ordinarily, gas targets fall into two categories: The first consists of a cell in which the gas is separated from the accelerator vacuum system by a very thin metallic foil (usually nickel or tantalum). But, when passing through the foil, an energy spread (straggling) of the charged particle beam results from a statistical variation of the number of ions formed by each particle in the foil. Even the thinnest vacuum tight foils introduce spreads as large as a few kev for Mev beams.

The second is the so called "differentially pumped chamber". The gas is allowed to escape into the vacuum system through the same orifice which admits the accelerated beam to the target chamber. To maintain accelerator vacuum, several high speed diffusion pumps must be employed along the beam tubing near the chamber. Thus it is very difficult to

localize a neutron source so that is has the small dimensions required for transmission of the neutrons through a collimator. Because of the radioactive nature of tritium, contamination of the vacuum system of the Van de Graaff seemed unavoidable with this target.

The original ideas from which the present target chamber evolved combine both nuclear and low temperature physics (Newson and Fairbank, 1958). The scheme was to provide two very cold surfaces whose temperatures could be separately controlled. A large quantity of tritium was to be deposited by condensation on one of the two surfaces. This surface was then to be heated so that the gas would evaporate and condense on the other surface. The proton beam was to pass through the vapor during its transit. Since the motion of the target gas would be mostly perpendicular to the beam direction relatively little of the gas could escape through the beam holes into the vacuum system and the Doppler effect would be minimized.

To provide sufficiently low temperatures for condensing tritium, we constructed a conventional cryostat capable of containing liquid helium. After several false starts, the above system was attached to the cryostat but testing with the $D^2(d, n)He^3$ reaction revealed that the loss rate into the vacuum system approached that expected for effusion of a directionally isotropic gas; this meant that the gas was no longer moving perpendicularly to the beam. Furthermore, to freeze out the necessarily large quantities of gas required a condensation time of several hours and the expenditure of a great deal of liquid helium, even when the gas was precooled to liquid

nitrogen temperatures. Consequently, we gave up the idea of shuttling the tritium, and developed a differentially pumped chamber in which cryogenic techniques eliminated the objections to this type of gas target, i.e., the pump was a liquid helium trap.

Since work with tritium is expensive and slightly hazardous, some sort of standin needed to be developed for the preliminary experiments. Deuterium, the most obvious choice, proved to be impractical so that we were forced to develop a rather flexible system on which the atomic and nuclear properties of several gases could be tested. After a number of trials, A^{40} was found to be well adapted to the atomic physics problems which make up a large part of this thesis.

CHAPTER II

APPARATUS

We will follow the path of the target gas in order to facilitate the description and explanation of the various parts of the gas handling system (Fig. 1) and the cryogenic target (Fig. 2). A cylinder feeds a reservoir whose volume far exceeds that of the gas lines. A manometer indicates the reservoir pressure which is maintained with a pressure regulator between the cylinder and reservoir. We can measure the flow rate of target gas by noting the drop in pressure when a valve between the regulator and the reservoir is closed. A needle valve allows the gas to bleed slowly into a purifier which consists of large bore tubing immersed in some suitable liquid coolant--liquid oxygen for argon. This procedure eliminates almost all the common contaminants which might condense in the more constricted passages of the gas line within the cryostat. From the purifyer, a long copper tube delivers the gas directly to the cryostat, except for a short section of tygon tubing for insulation.

We did not intend originally to make absolute measurements on the flow rate of the gas. However, it later turned out to be our only useful

Figure 1. Schematic Diagram of Cryostat and its Gas Handling System

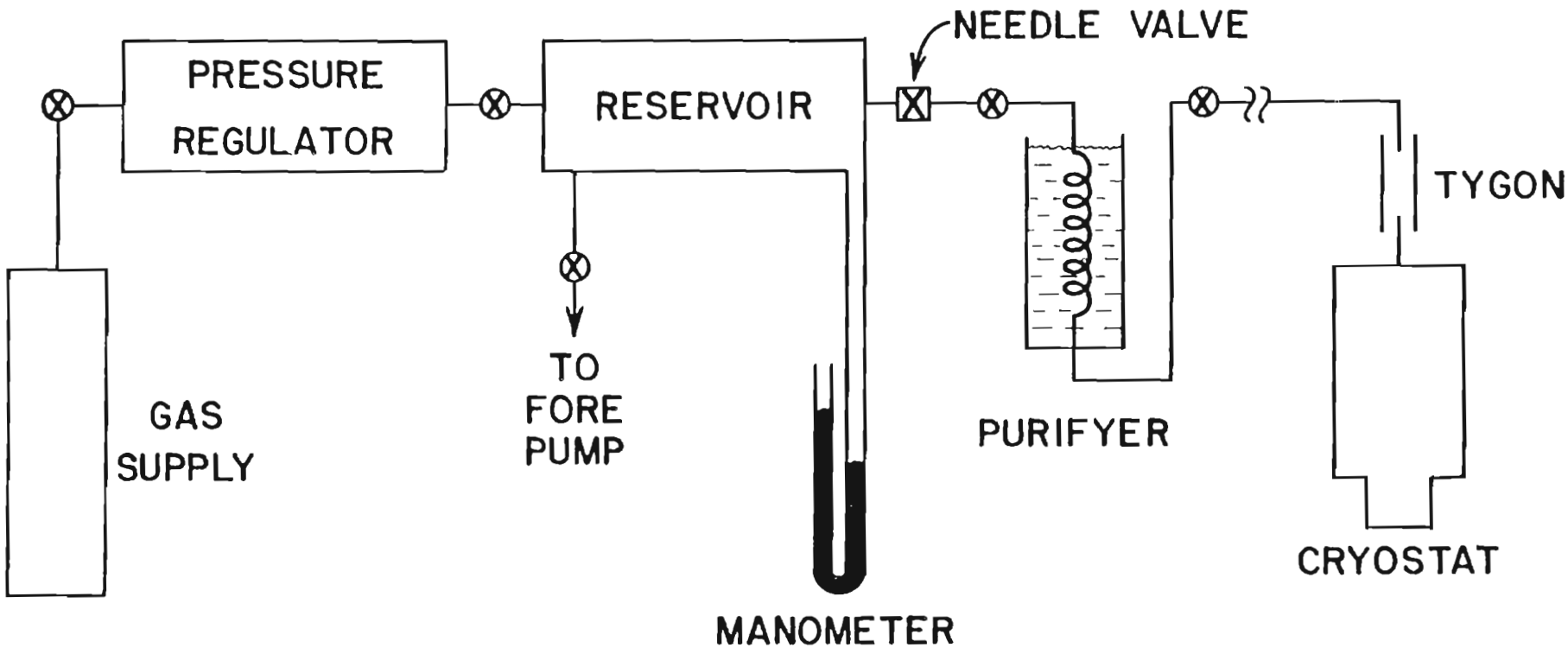

⊗ ISOLATION VALVE

GAS HANDLING SYSTEM

Figure 2. The Cryogenic System. Cryostat and Appended Target Chamber.

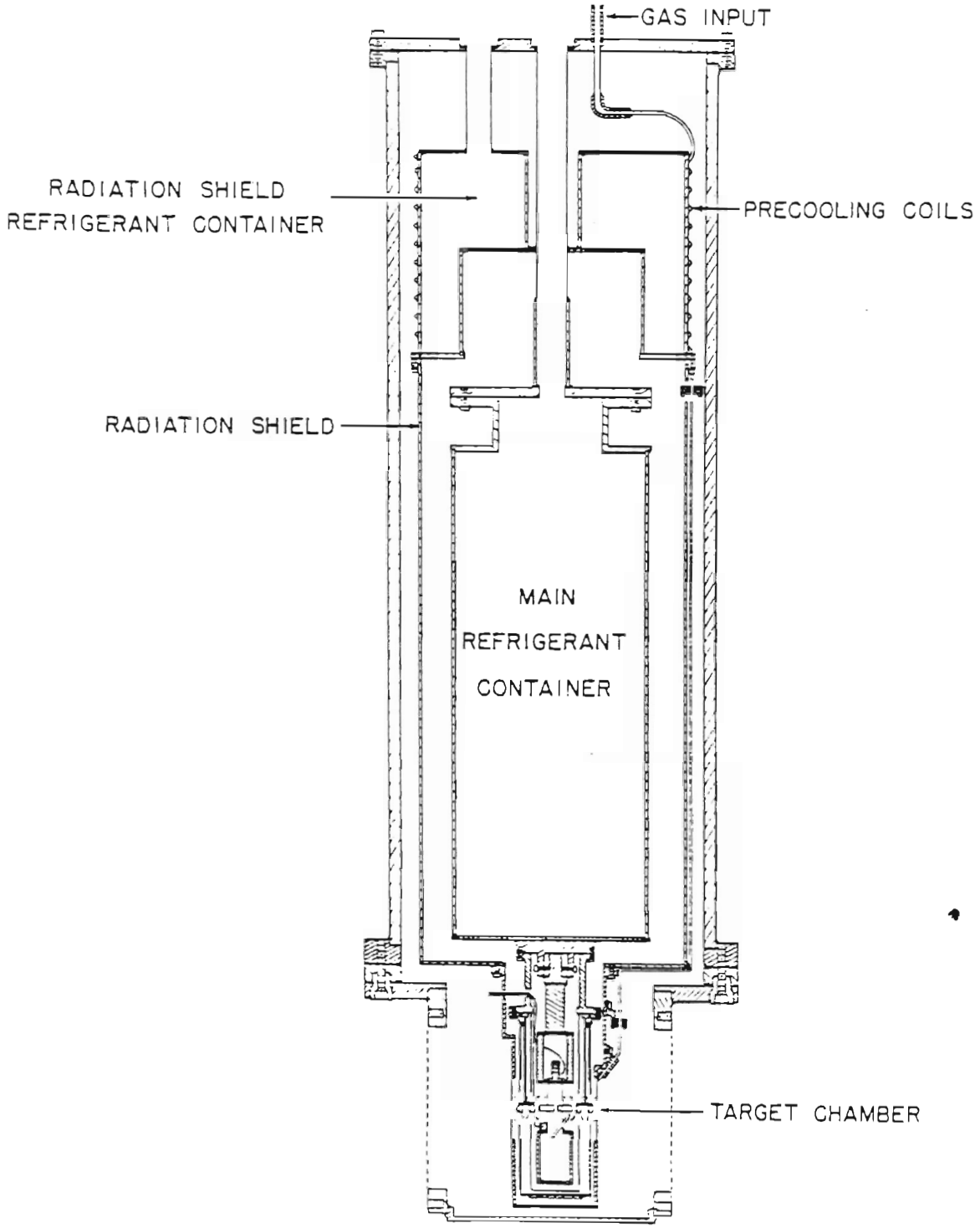

CRYOGENIC GAS TARGET

measure of the density of the target gas. We found that the flow rate gives us a means of reproducing target densities within ±10%. This was verified by observing a prominent pair of resonances in the $A^{40}(p, n)K^{40}$ reaction (2.462 Mev) for several days in a row. We found the neutron yield to be proportional to the flow rate in the interval 7cc/min to 20cc/min. Absolute densities must be calculated from yields and known cross sections.

Our cryostat is capable of containing all the commonly used liquid refrigerants, including liquid helium at 4.2°K. Thermal radiation is an acute problem in containing liquid helium. Because of its high reflectivity in the infrared region, we have chosen to make all the liquid containers of copper. Even so, it is still necessary to surround the main refrigerant container with a radiation shield. Ordinarily, if liquid helium is the main refrigerant, liquid nitrogen is used to cool the radiation shield. Thermal radiation from a surface at 77°K is an order of magnitude less than the heat conduction down the stainless steel support tubes.

However, the target gas will ultimately be condensed on a surface in direct contact with the main refrigerant. This contribution to the boiling rate of the liquid helium is a function of the specific heat, the heats of vaporization and fusion (or sublimation), and the rate at which the gas is introduced into the target chamber. For argon, gas flow constitutes the most serious source of heat input. To minimize this heat input we have soldered a pre-cooling copper coil to the radiation shield refrigerant container. Thus, the radiation shield coolant is chosen for having a boiling

point as close as possible to that of the target gas. In the case of argon, liquid nitrogen was precluded since we feared further constriction due to condensation in the gas line. We used liquid oxygen which proved to be quite suitable even though the boiling point of argon was slightly lower than that of oxygen.

In Fig. 3 we see an enlarged section of the lower part of the cryogenic system. Inside the extension of the radiation shield, we see the target chamber proper which is appended to the main refrigerant container. This chamber consists of three different, coaxial, cylindrical shells, all of which are in direct thermal contact with the liquid helium. The innermost unit comprises those parts labeled "cooling cavity", "thermometer", "reaction tubes", "heater", and "temperature gradient rod". All those parts below the stainless steel "temperature gradient rod" are made from high conductivity materials to insure that uniform temperature is attained. The material and dimensions of the "temperature gradient rod" are very important; the manner in which they are chosen will be discussed later in this chapter.

The gas enters the target chamber via the stainless steel "capillary tube" and rapidly attains the temperature of the walls of the "cooling cavity". It then diffuses into the vicinity of the "reaction tubes" where the target gas is bombarded by the proton or deuteron beam. The chamber and "reaction tubes" are made from 0.001" silver foil to minimize neutron scattering. Since our target is windowless, there is nothing to prevent the escape of

Figure 3. Enlargement of the Target Chamber

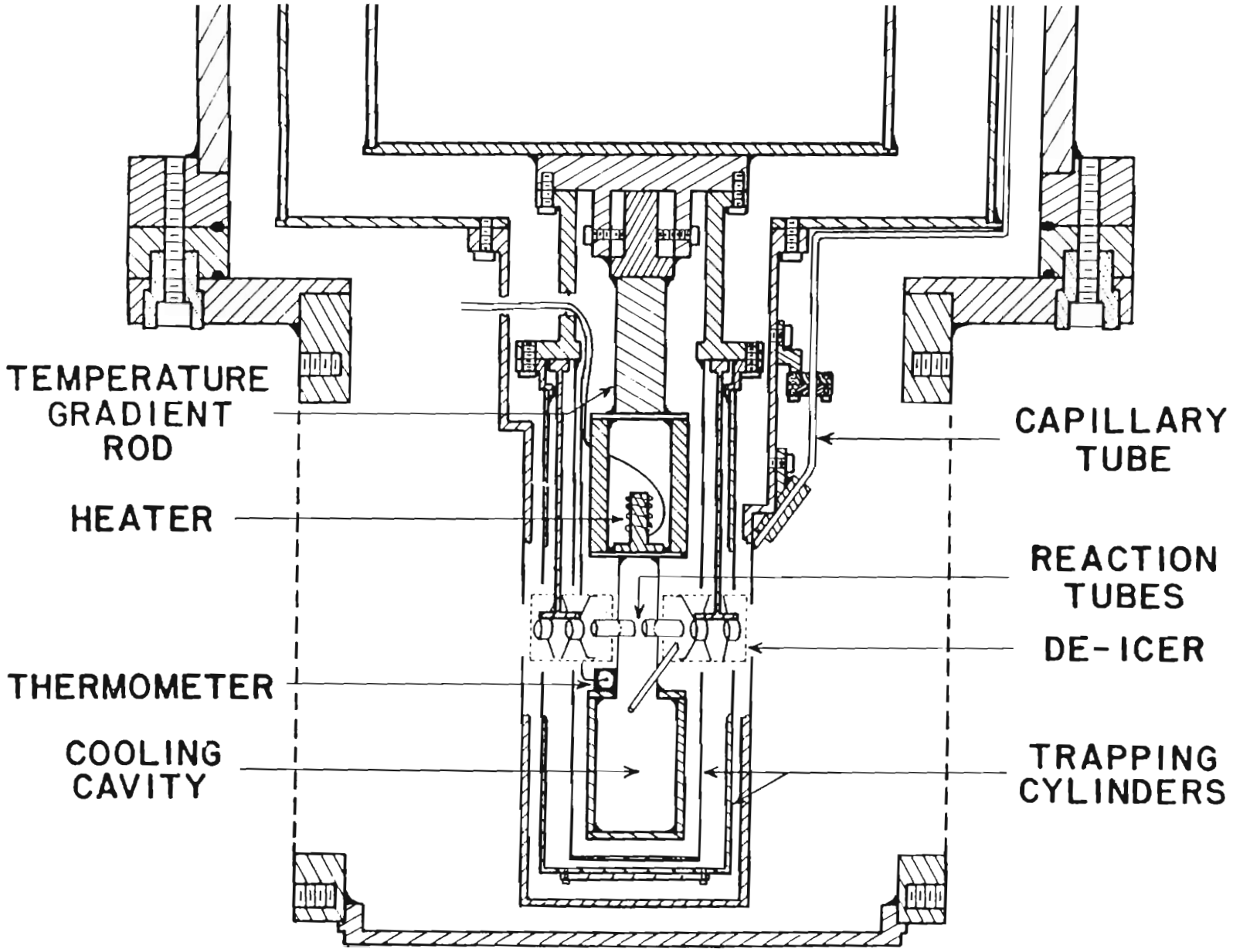
TEMPERATURE GRADIENT ROD
HEATER
THERMOMETER
COOLING CAVITY
CAPILLARY TUBE
REACTION TUBES
DE-ICER
TRAPPING CYLINDERS

the gas from this unit. The "reaction tubes" (Herb, 1961) do, however, slow down the escape of the gas by about a factor of three relative to the effusion rate through holes of the same diameter.

The operating procedure for the cryogenic target chamber is quite simple. Gas is bled in through the capillary into the "cooling cavity" at a steady rate. We maintain the temperature of the cooling cavity and the reaction tubes well above a minimum temperature necessary to prevent condensation in this area. It is possible to estimate this minimum temperature from kinetic theory, as follows. First, we ignore the presence of the holes in the target chamber and assume that the target consists of a vapor in equilibrium with any condensate. This vapor pressure, as a function of the temperature, is known for most useful gases and we shall designate it p_1. Clausing has shown that the escape rate of a gas through a tube of length L and radius R is given by (Loeb, 1934)

$$n = P(p_1-p_2)(M/2\pi R_o T)^{1/2} a/m \quad \text{molecules/sec}$$

where "m" = mass of molecule, "p_2" = pressure at opposite end of tube which for our case is assumed zero, "M" = molecular weight, and "a" is the cross section of the tube. "P" is a parameter which varies from 1.0 at L/R = 0 to 8R/3L when $L/R = \infty$. The tubes presently in use have L/R = 5 and P = .31. It should be pointed out that this relation is valid only as long as the mean free path of the gas is longer than the dimensions of the escape tubes. When this limit is exceeded the escape rate becomes smaller than the above relation would indicate.

Knowledge of the rate at which we push the gas into the target chamber, allows us to estimate the temperature at which the gas can escape at the same rate. Obviously, since this type of calculation is approximate, we must allow a considerable safety margin; thus, we usually maintain the target temperature somewhat above this "equalization point"--10° to 15° in the case of argon. Under this condition, we were able to verify that no condensation took place in the reaction tubes since it could be seen with the telescope used in the beam alignment procedure, as is discussed in the next chapter.

As is apparent in the above discussion, it is quite necessary to be able to measure and also maintain the temperature of the entire unit located below the temperature gradient rod. The "thermometer" is simply a 1/2 watt carbon resistor whose resistance has been calibrated against a series of known temperatures: room temperature, 77°K for liquid nitrogen, several points above the boiling point of liquid hydrogen, and 4.2° for liquid helium. For interpolation the formula

$$\mathrm{Log}_{10}R + K/\log_{10}R = A + B/T$$

is used (Clement and Quinnell, 1952).

The temperature is monitored by observing the resistance of the thermometer with a Wheatstone bridge. Because of the degree of precision originally thought to be necessary, a rather complicated design, based on Dessler's bridge (1956) which operated at 10 cps, was employed--see Fig. 4. Basically, the electronics consists simply of a 10 cycle

Figure 4. Schematic Circuit Diagram for Temperature Indicator

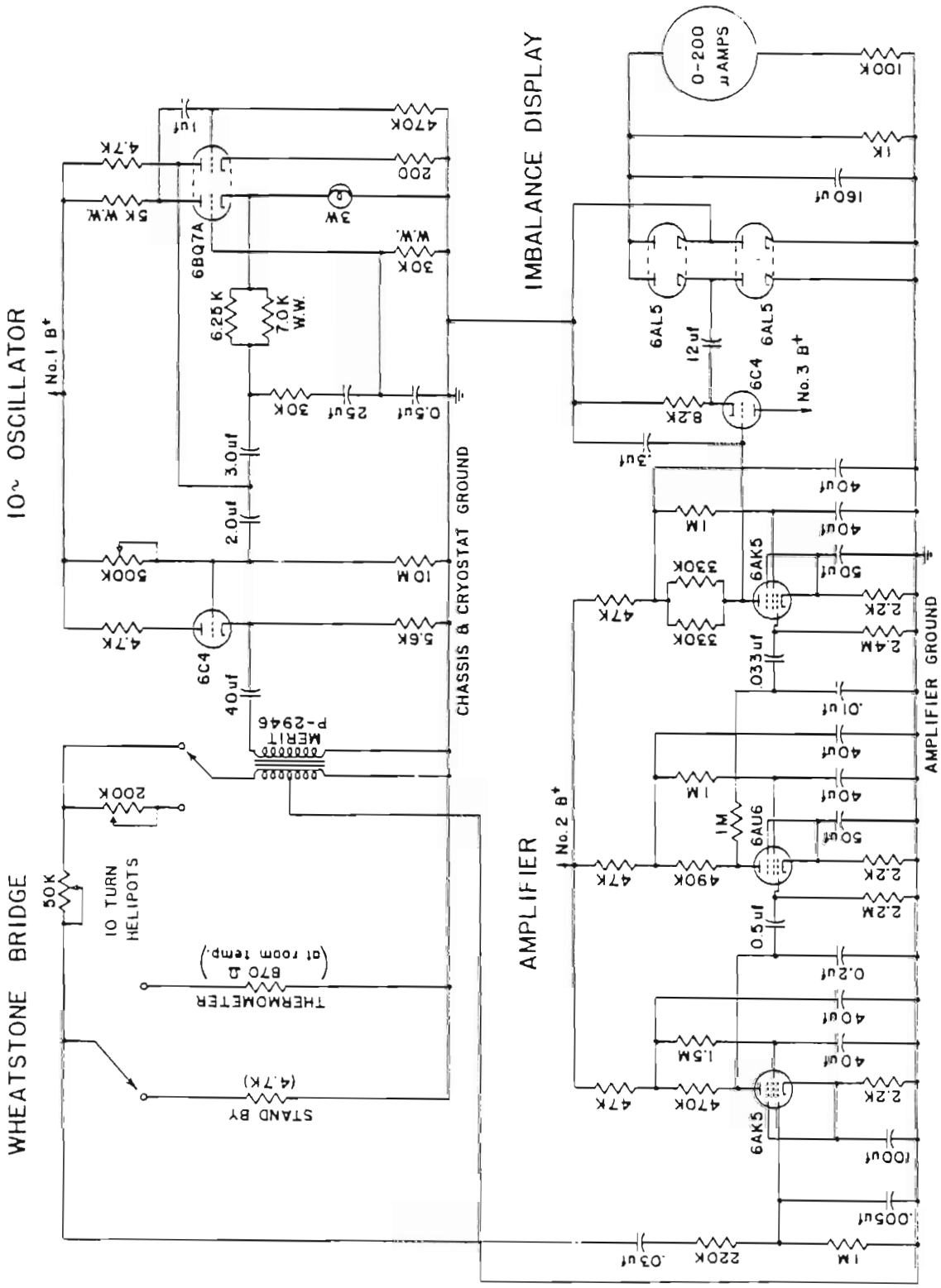
TEMPERATURE INDICATOR
WHEATSTONE BRIDGE
10~ OSCILLATOR
IMBALANCE DISPLAY
AMPLIFIER
CHASSIS & CRYOSTAT GROUND
AMPLIFIER GROUND
No.1 B+
No.2 B+
No.3 B+
0-200 μAMPS
6BQ7A
6C4
6AL5
6AU6
6AK5
MERIT P-2946
10 TURN HELIPOTS
THERMOMETER
STAND BY
(4.7K)

oscillator which feeds the primary winding of a transformer. The center tap of the secondary winding is the chassis ground, thus two arms of the Wheatstone bridge are formed by the divided secondary winding with the oscillating voltage impressed across both of them. A minimum signal enters the amplifier when the potentiometer is adjusted to match the resistance of the thermometer. Any mismatch signal is amplified and then rectified for D.C. display on a meter. The vernier of the 10 turn helipot potentiometer thus indicates the temperature when the meter reading is minimized.

The temperature can be maintained at the desired level simply by applying a D.C. potential across the wire wound coil of the "heater". In order to avoid having to supply an undue amount of heat, we carefully adjust the material and dimensions of the "temperature gradient rod" so that the gas flow itself will warm the target chamber to within a few degrees of the desired temperature. Obviously, no single rod can suit all target gases. For argon, stainless steel is satisfactory, but for deuterium we had to substitute a thin wall tube of silver. The dimensions are generally adjusted empirically.

We now come to that feature of the cryogenic target chamber which we feel is by far the most important. Thus far, our chamber is just like any other differentially pumped chamber, with the exception of the temperature control problem. All windowless gas chambers face a common difficulty which has heretofore limited the minimum target density--namely

the problem of removing the gas from the vacuum system. However a cryostat is, by its very nature, a "cold trap", and surfaces at liquid helium temperatures provide about the most effective pumping action possible. We have provided these surfaces by surrounding the innermost unit with two concentric "trapping cylinders" in which the only escape path is the small solid angle subtended by the beam holes.

After leaving the "reaction tubes", most of the target gas condenses upon the "trapping cylinders". Of course, as long as we operate the chamber, the condensed solid will tend to grow inward from the edges of the beam holes. The result is a solid target of great thickness, which has a yield far greater than the neutron production in the "reaction tubes". Thus, we have installed along the beam path two "de-icer" systems to eliminate this problem. The assembly consists of baffles and a thin wire mesh which is mounted, along with a resistance heater, on a stainless steel rod which is in thermal contact with the main refrigerant reservoir. In practice we heat the "de-icers" just enough to prevent any condensation in the beam path.

CHAPTER III

EXPERIMENTAL CONDITIONS

Since there are problems associated with handling radioactive tritium (2,400 curies/liter) we decided to find some stable element in gaseous form with which we could estimate the thinness of the target in the cryogenic chamber. Because neutron detectors of high efficiency were either already available or easy to build, we concentrated on (p, n) and (d, n) reactions. The first experiment involved using the $H^2(d, n)He^3$ reaction, with the 20^o neutron spectrometer, in an attempt to observe the neutron production. While there were definite indications that the expected behavior occurred, quantitative measurements were rendered quite difficult because of the highly penetrating background neutrons associated with a deuteron beam.

The $B^{11}(p, n)C^{11}$ reaction, with research grade BF_3 as the target gas, was then observed with the same 20^o spectrometer. The threshold of this reaction offered a means of estimating the average energy loss within the target. Unfortunately, these experiments were performed on the 4 Mev Van de Graaff accelerator during a period in which its corona stabilizer

and belt charging systems were not functioning efficiently. However, for the first time, we felt we had proof that a target thinner than 600 ev had been formed. Since that time, this experiment has been repeated by Mr. P. M. Beard (1962) under more favorable conditions; his analysis is still in progress.

At this point Dr. R. M. Williamson (1962) suggested that we try the $A^{40}(p, n)K^{40}$ reaction since we feared that molecular vibration in the BF_3 molecule might perhaps cause an effective energy spread (a Doppler effect) which could mask the properties of a thin target. The monatomic argon eliminated this concern. At neutron threshold, the excitation energy of the compound K^{41} nucleus is about 11 Mev. Since both N and Z (the neutron and proton numbers respectively) of the target nucleus are twice removed from the magic number 20, the spacing between neighboring levels should be small (Newson and Rohrer, 1954). Fortunately the high spin of the residual nuclear ground state ($J^{\pi} = 4^-$) (Davis, Nagle, and Zacharias, 1949) has the effect of making the most probable observed resonances quite narrow. Thus the true widths of some of the resonances should be so narrow that the apparent width is a direct measurement of the thickness of targets in the cryogenic chamber.

Most components of the experiment are summarized in Fig. 5, a schematic representation of the floor plan. The proton beam was supplied by the 3 Mev Van de Graaff Accelerator which was built by the High Voltage Engineering Corporation and installed in July, 1961. One of the earliest

Figure 5. Floor Plan of Both $A^{40}(p, n)$ and $B^{11}(p, n)$ Experiments

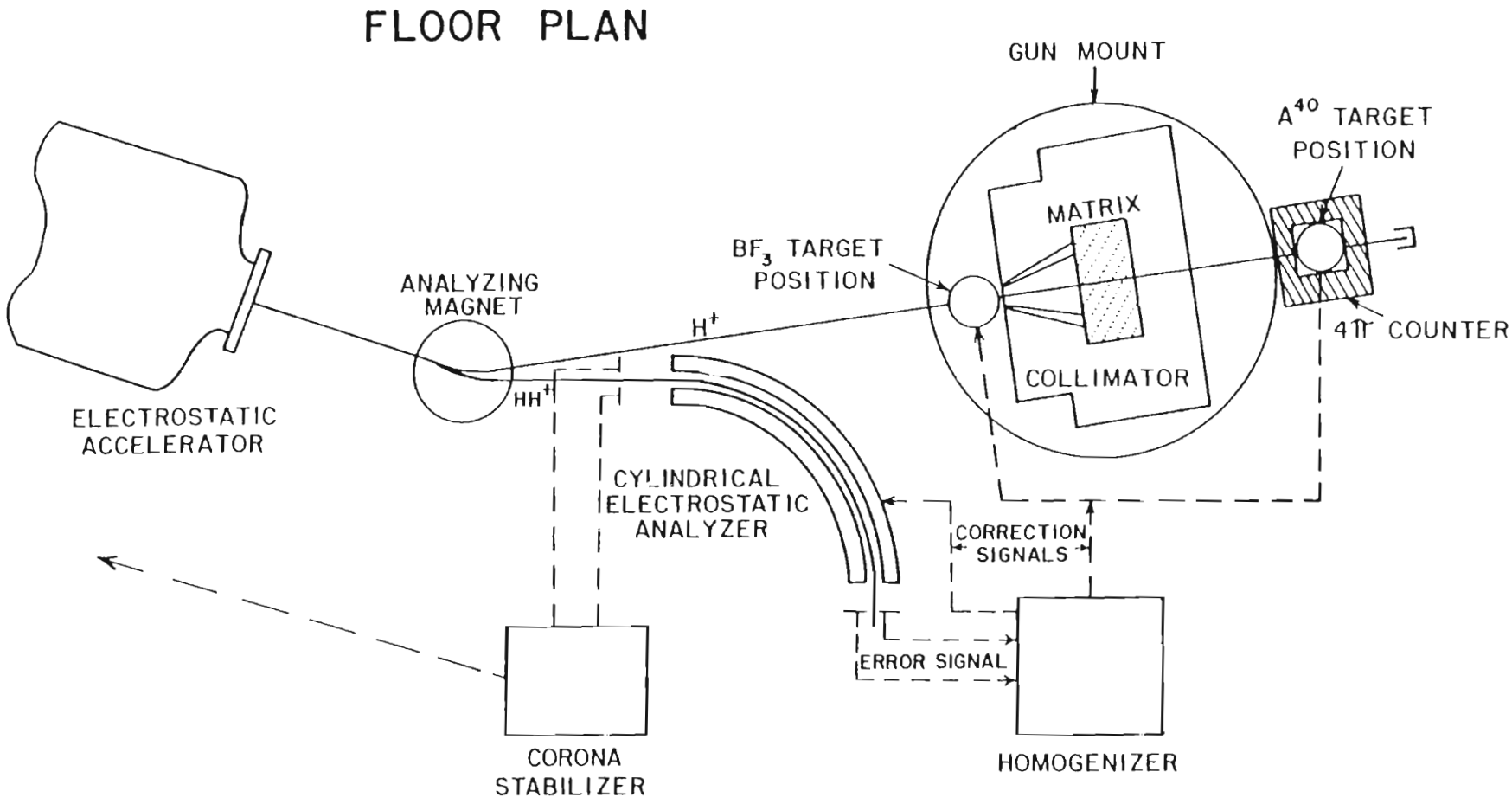
FLOOR PLAN
GUN MOUNT
A40 TARGET POSITION
MATRIX
BF3 TARGET POSITION
ANALYZING MAGNET
H+
HH+
4π COUNTER
COLLIMATOR
ELECTROSTATIC ACCELERATOR
CYLINDRICAL ELECTROSTATIC ANALYZER
CORRECTION SIGNALS
ERROR SIGNAL
CORONA STABILIZER
HOMOGENIZER

experiments on this machine was a measurement of the resolution of the controlled accelerated beam, after magnetic analysis. A thick target study of the $C^{13}(p,\gamma)N^{14}$ resonance at 1.746 Mev indicated a resolution a little better than 1/4000 at optimum adjustment (Kyker and Williamson, 1962). The only parameter which seemed to be critical was the sensitivity of the corona stabilizer system. An insulated plate is mounted within the pressure vessel near the high voltage terminal of the accelerator. The ripple of the terminal is induced on this plate and displayed on an oscilloscope. It is possible to adjust the corona control sensitivity for best resolution by minimizing the fluctuations of the oscilloscope pattern.

Several years ago we developed an electronic device, called the "homogenizer" to counteract the low frequency fluctuation of the accelerator potential (Parks et al., 1958). The beam is first passed through a modified 90° cylindrical electrostatic analyzer, (Warren, Powell, and Herb, 1947) in which nearly all the deflecting voltage is placed on the inner plate. A potential fluctuation then shows up as a lateral position shift of the beam at the image slit. We then use the image slits of the analyzer as the source of error signal, "slit signal", which is fed to the homogenizer. The two slit signals are subtracted in a difference amplifier and the output then drives a triode which operates around an average plate voltage of +3500. A voltage divider feeds the fraction 1/111 of this plate voltage fluctuation back to the outer plate of the electrostatic analyzer. This ratio insures that the outer deflector plate voltage will change just

enough to force the proton beam through the middle of the image slits. The plate of the triode is tied directly to the target chamber, and since the target voltage is equal in magnitude but exactly 180° out of phase with the original energy shift, the effective proton energy relative to the target remains constant. Because of the feedback property there is no necessity for constant gain which is so difficult to obtain in a direct coupled amplifier.

The $C^{13}(p,\gamma)$ experiment was repeated by Mr. P. M. Beard and Mr. C. C. Kyker, Jr. (1962) to see if use of the homogenizer would materially decrease the effective beam spread below the disappointing value of 300 ev previously reported. It was found that a spread of 100 ev (1/16,000) was not inconsistent with the data. However, they could not claim the above figure due to the uncertainty in estimating the Doppler effect in a graphite target. Further demonstration of small beam spread had to wait until the discovery of the very narrow resonances in the $A^{40}(p,n)$ studies. It is surmised that this great improvement over the 4 Mev machine experience is due to the improved belt charging and corona control systems with which the 3 Mev machine is equipped.

In the same paper that described the "homogenizer", a "two part system" was also reported. Instead of using the beam that goes through the electrostatic analyzer, we take advantage of the fact that an HH^+ beam accompanies the H^+ beam and that the two are separated by the magnetic analyzer. Thus we can use the HH^+ beam to obtain our correction signal for the H^+ beam without suffering any of the usual control and resolution

slit losses. We were usually able to deliver 20 to 30 microamperes at optimum resolution to the first of a series of proton beam collimators (necessary only for beam definition).

Proton beam definition presented us with one of our most difficult problems. The diameter of the reaction tubes was only 0.125" and it was absolutely necessary that no primary or scattered beam of any consequence should strike these tubes. One obvious reason is the possibly large heat input to the target chamber. More important is the large yield of energetically heterogeneous neutrons from impurities on the tube walls. To complicate matters, thermal contraction changes the vertical position of the target chamber when the cryostat is filled with the main refrigerant.

To make sure that no beam strikes the reaction tubes, we have constructed a proton beam collimator which consists of a series of four diaphragms ranging from .0625" farthest from the target chamber to .0830" at the closest distance. This arrangement insures that protons scattered from the smallest aperture cannot strike any surfaces at low temperatures. To monitor the alignment, we measure the beam striking the insulated diaphragm closest to the "reaction tubes". Ordinarily we can reduce the apparent beam striking the last collimator to less than .005 microamperes. To allow use of intense beams, the initial collimating diaphragms are water cooled.

To show that the above procedure insured good alignment, we performed the following experiment. A neutron background measurement with the beam passing through the chamber was made prior to allowing gas

into the cryostat. The target chamber was then operated for approximately two hours at a high yield energy with the normal gas flow. The gas was then shut off but all other electric controls remained as during the run. After about five minutes the neutron yield returned to the original background level. Again the target chamber was operated under normal conditions, but this time we shut off the electric controls, as well as the gas flow, at the end of two hours. The neutron yield again returned to the original background level. Had there been any condensation on the reaction tubes, and had there been any appreciable scattered or direct beam striking the inner walls of these tubes, a large increase over background should have been noted.

Through liberal use of brass bellows we were able to move the front end of the rigid proton collimator structure about a pivot point just in front of the last diaphragm. Thus by a process of adjusting both the beam position, through magnetic deflection, and the collimator alignment, we could attain the desired minimum beam on the last collimator. A small light bulb was placed within the cryostat, which allowed a visual check on the alignment. This was accomplished by looking through a clear lucite window on the rear end of the beam collector housing. A telescope made possible very accurate adjustments of the collimator with respect to the target chamber position. Ordinarily beam alignment was accomplished with the cryostat at room temperature. A large bellows, coaxial with the beam line, connects the proton beam collimator to the cryostat base. Thus we

can readjust the reaction tube position after the cooling down contraction has ceased.

In order to obtain the maximum possible yield we have constructed a neutron detector which subtends a solid angle of approximately .93(4π) steradians. BF_3 counters are inserted in two separate halves of a matrix constructed of polyethylene strips. These two halves vertically surround the cryostat with the target centered vertically and horizontally. We have checked the response of one of the two halves and have found that it is at least as flat as the response of the McKibben long counter (Hansen and McKibben, 1947) in the neutron energy interval 5 to 150 kev, with an efficiency of the order of 10%.

Since our detectors were totally unshielded, we decided to place the target chamber on the back side of the large 6' x 7' x 10' water tank which ordinarily shields the 20° - 160° neutron collimator. The accelerator, magnet, cylindrical analyzer, and their associated slit systems were all effectively shadowed from the counters by this tank.

CHAPTER IV

RESULTS

A. Yield of the $A^{40}(p, n)K^{40}$ Reaction

In Figures 6, 7 and 8 we show the observed total yield of the $A^{40}(p, n)K^{40}$ reaction as a function of the proton energy. This data was taken with the unshielded 0.93 (4π) detector. No correction has been made for background which was generally $\lesssim$ 60 neutron counts per microcoulomb of proton current. The point scatter seems no worse than expected from statistical fluctuations. We found that about one half of our background was present even when the proton beam was stopped before the large water tank. The other half seemed to come from the proton beam collimator just in front of the target chamber. Since this collimator was so close to the cryostat, it was impossible to place any effective shielding between the collimator and the 4π counter. Nevertheless background presents no difficulty in analysis of any but the smallest resonances.

In the vicinity of a resonance peak, our data has been taken in 50 ev steps, i.e., about one third of our estimated effective proton beam spread. Fortunately, with the homogenizer it is not necessary to adjust

Figure 6. The $A^{40}(p, n)$ Yield as a Function of the Proton Energy, E_p

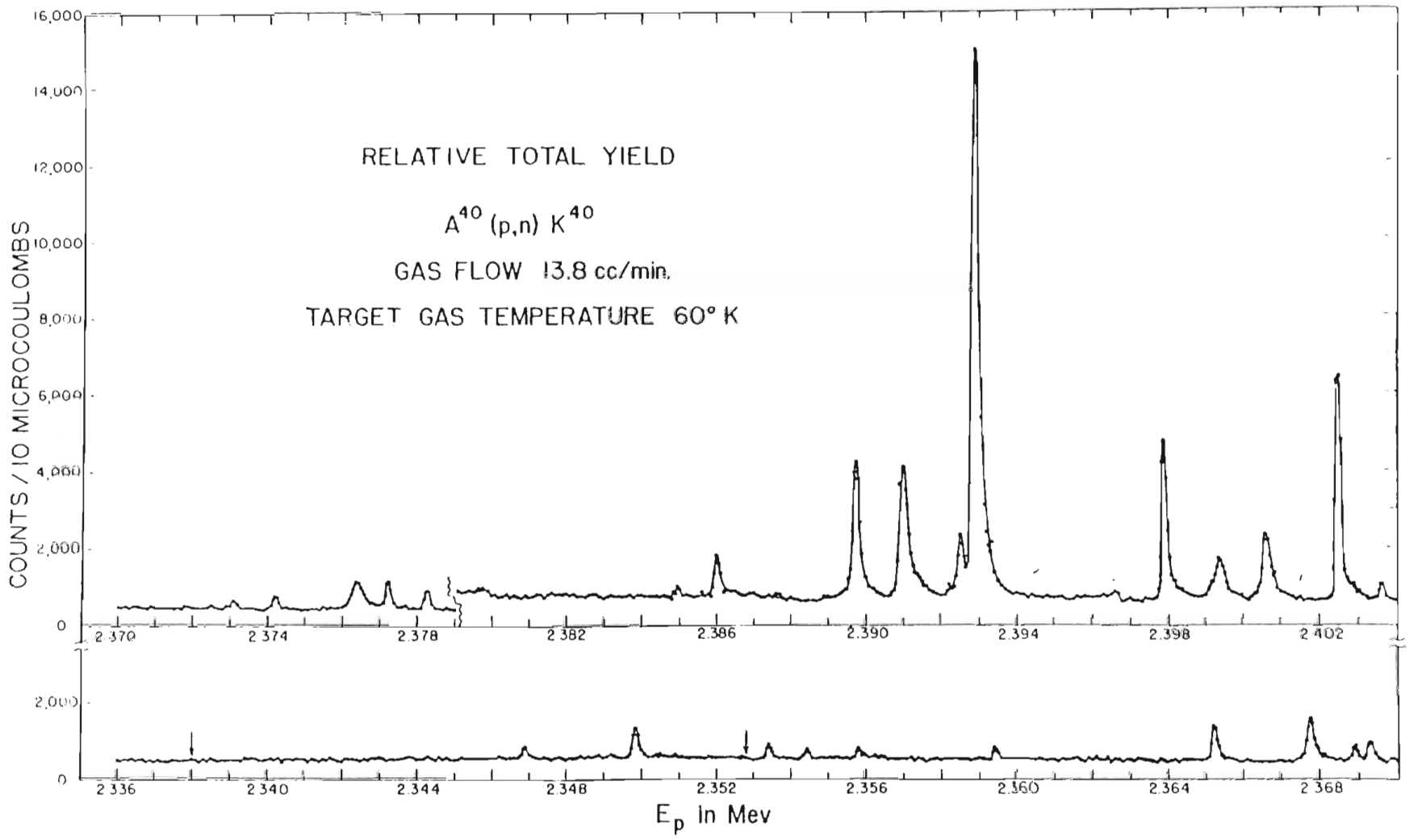
RELATIVE TOTAL YIELD
A40 (p,n) K40
GAS FLOW 13.8 cc/min.
TARGET GAS TEMPERATURE 60° K
COUNTS / 10 MICROCOULOMBS
16,000
14,000
12,000
10,000
8,000
6,000
4,000
2,000
0
2.370
2.374
2.378
2.382
2.386
2.390
2.394
2.398
2.402
2,000
0
2.336
2.340
2.344
2.348
2.352
2.356
2.360
2.364
2.368
Ep In Mev

Figure 7. Continuation of $A^{40}(p,n)$ Yield

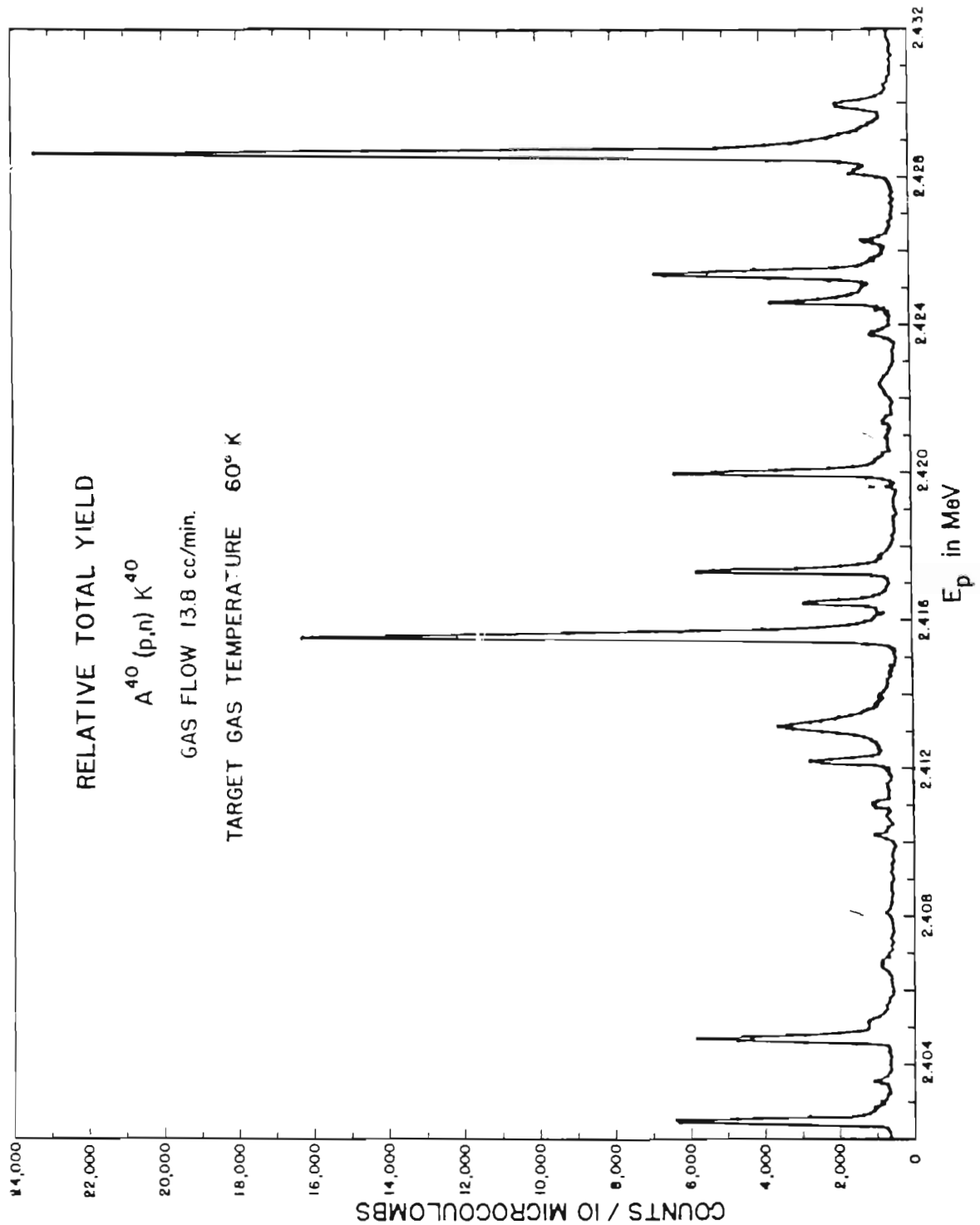
RELATIVE TOTAL YIELD
A^{40} (p,n) K^{40}
GAS FLOW 13.8 cc/min.
TARGET GAS TEMPERATURE 60° K
COUNTS / 10 MICROCOULOMBS
0
2,000
4,000
6,000
8,000
10,000
12,000
14,000
16,000
18,000
20,000
22,000
24,000
2.404
2.408
2.412
2.416
2.420
2.424
2.428
2.432
E_p in MeV

Figure 8. Continuation of $A^{40}(p, n)$ Yield

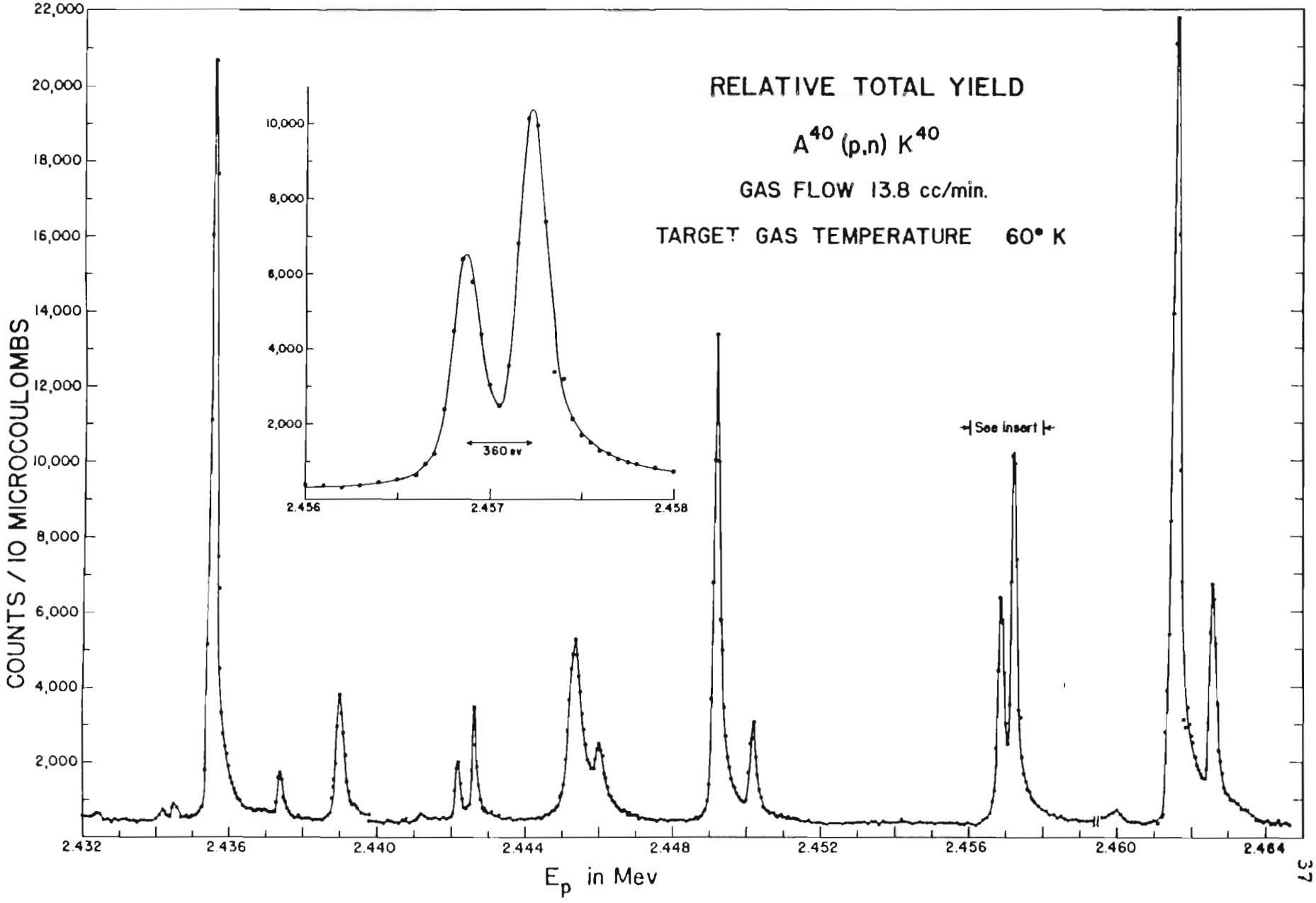
RELATIVE TOTAL YIELD
A^{40} (p,n) K^{40}
GAS FLOW 13.8 cc/min.
TARGET GAS TEMPERATURE 60° K
COUNTS / 10 MICROCOULOMBS
E_p in Mev
See insert
360 ev
22,000
20,000
18,000
16,000
14,000
12,000
10,000
8,000
6,000
4,000
2,000
2.432
2.436
2.440
2.444
2.448
2.452
2.456
2.460
2.464
10,000
8,000
6,000
4,000
2,000
2.456
2.457
2.458

both the electrostatic analyzer and the deflection magnet current (which controls the accelerator potential through the corona control slit system) with every small change in energy. Assume that the average machine energy is within $\pm$500 ev of the value necessary to pass through the center of the image slits of the cylindrical analyzer in the absence of the homogenizer. The average difference of the machine potential and the corresponding cylindrical analyzer setting is placed on the target through the homogenizer. The result is that the effective proton energy at the target is just that of the analyzer setting. Thus, as long as the difference between the machine energy and the analyzer setting is within the range of linear performance of the homogenizer (average target voltage 3000 to 4000), we can change the effective proton energy only by changing the analyzer high voltage.

The first resonance in the data appears at 2.3466 $\pm$ 0.001 Mev. For an interval of about 40 kev only very small resonances are observed. However at approximately 2.390 Mev we begin to see much larger peak yields which may be related to the threshold of the second neutron group of the A^{40}(p, n) reaction. The most prominent peaks are above background by two orders of magnitude, while the widths are never greater than 450 ev. There does seem to be an uncommonly large number of apparent doublets but no special significance can now be attributed to them. However, to demonstrate the very low effective energy spread available with this cryogenic system, we have expanded the doublet at 2.457 Mev and show it in

the insert of Fig. 8. Here, two resonances about 200 ev wide and only 360 ev apart are clearly resolved. In Table 1 we have listed the resonance energy, widths at half maximum for each observed peak, relative integrated yields, and nearest neighbor spacing. A histogram of the observed half widths of those resonances which are intense enough to estimate the width to within ± 10 ev is shown in Fig. 9. This apparent width must depend almost entirely on the effective proton energy spread for the narrow resonances but probably is close to the true width (Γ) for the largest.

B. Interpretation

1. Efficiency of Cryogenic Differential Pumping.

We can estimate how well the trapping cylinders reduced the pressure of argon outside of the target chamber by taking advantage of the fact that the target chamber potential is, on the average, about 3.5 kilovolts higher than that of the surrounding beam tubing. The amount of grounded beam tubing on either side of the 4π counter is about three feet. The section closest to the large neutron collimator tank is evacuated with a small (50 liter/sec) Hg diffusion pump, but the section leading to the beam collector has no such pump. Thus the density of target molecules in this section might have been great enough to constitute a target at a potential 3.5 kilovolts lower than the target chamber. We see (Fig. 8) prominent resonances at 2.457 and 2.462 Mev. If the density of argon

Table I. Experimentally Observed Resonance Properties

Res. No.	Proton Energy	Apparent Half Width	Relative Integrated Yield	Local Spacing
1	2.4624 Mev	200 ± 10 ev	.308	
2	2.4615	200 ± 10	1.096	.9 kev
3	2.4600	300 ± 50	.017	1.5
4	2.4572	210 ± 10	.562	2.8
5	2.4569	200 ± 10	.285	.3
6	2.4502	250 ± 10	.153	6.7
7	2.4492	180 ± 10	.678	1.0
8	2.4460	250 ± 10	.083	3.2
9	2.4454	440 ± 10	.661	.6
10	2.4426	140 ± 10	.122	2.8
11	2.4422	180 ± 10	.059	.4
12	2.4412	250 ± 50	.008	1.0
13	2.4390	240 ± 10	.208	2.2
14	2.4374	180 ± 10	.062	1.6
15	2.4356	190 ± 10	1.042	1.8
16	2.4345	210 ± 10	.016	1.1
17	2.4342	210 ± 10	.013	.3
18	2.4325	200 ± 50	.013	1.7
19	2.4300	300 ± 10	.110	2.5
20	2.4236	190 ± 10	1.239	1.4
21	2.4231	280 ± 50	.056	.7

Table 1 (continued)

Res. No.	Proton Energy	Apparent Half Width	Relative Integrated Yield	Local Spacing
22	2.4263	200 ± 10	.039	1.8
23	2.4254	250 ± 10	.369	.9
24	2.4247	210 ± 10	.159	.7
25	2.4238	200 ± 10	.025	.9
26	2.4225	300 ± 50	.019	1.3
27	2.4214	200 ± 50	.010	1.1
28	2.4210	250 ± 50	.014	.4
29	2.4200	170 ± 10	.246	1.0
30	2.4196	120 ± 50	.005	.4
31	2.4173	170 ± 10	.219	2.3
32	2.4164	190 ± 10	.123	.9
33	2.4156	200 ± 10	.734	.8
34	2.4132	420 ± 10	.334	2.4
35	2.4122	190 ± 10	.098	1.0
36	2.4110	280 ± 50	.031	1.2
37	2.4102	160 ± 50	.017	.8
38	2.4081	200 ± 50	.007	2.1
39	2.4067	350 ± 50	.018	1.4
40	2.4049	320 ± 50	.031	1.8
41	2.4044	180 ± 10	.223	.5

Table 1 (continued)

Res. No.	Proton Energy	Apparent Half Width	Relative Integrated Yield	Local Spacing
42	2.4031	180 ± 10	.018	1.3
43	2.4022	200 ± 10	.251	.9
44	2.4003	240 ± 10	.147	1.9
45	2.3990	300 ± 10	.089	1.3
46	2.3976	180 ± 10	.192	1.4
47	2.3966	300 ± 50	.011	1.0
48	2.3926	240 ± 10	.790	4.0
49	2.3922	230 ± 50	.078	.4
50	2.3919	120 ± 50	.007	.3
51	2.3907	260 ± 10	.220	1.2
52	2.3894	200 ± 10	.185	1.3
53	2.3857	140 ± 10	.047	3.7
54	2.3846	110 ± 10	.006	1.1
55	2.3780	200 ± 10	.016	6.6
56	2.3770	180 ± 10	.031	1.0
57	2.3762	400 ± 10	.061	1.2
58	2.3741	180 ± 10	.014	2.1
59	2.3729	170 ± 10	.009	1.2
60	2.3689	200 ± 10	.024	4.0
61	2.3686	160 ± 10	.016	.3

Table 1 (continued)

Res. No.	Proton Energy	Apparent Half Width	Relative Integrated Yield	Local Spacing
62	2.3675	210 ± 10	063	1.1
63	2.3649	170 ± 10	038	2.6
64	2.3591	150 ± 10	.010	5.8
65	2.3555	170 ± 10	.014	3.6
66	2.3542	140 ± 10	.006	1.3
67	2.3531	180 ± 10	.013	1.1
68	2.3496	180 ± 10	.028	3.5
69	2.3466	150 ± 10	.009	3.0

Figure 9. Histogram of Apparent Widths at Half Maximum. Only those for which probable errors are $\pm$ 10 ev or less are included.

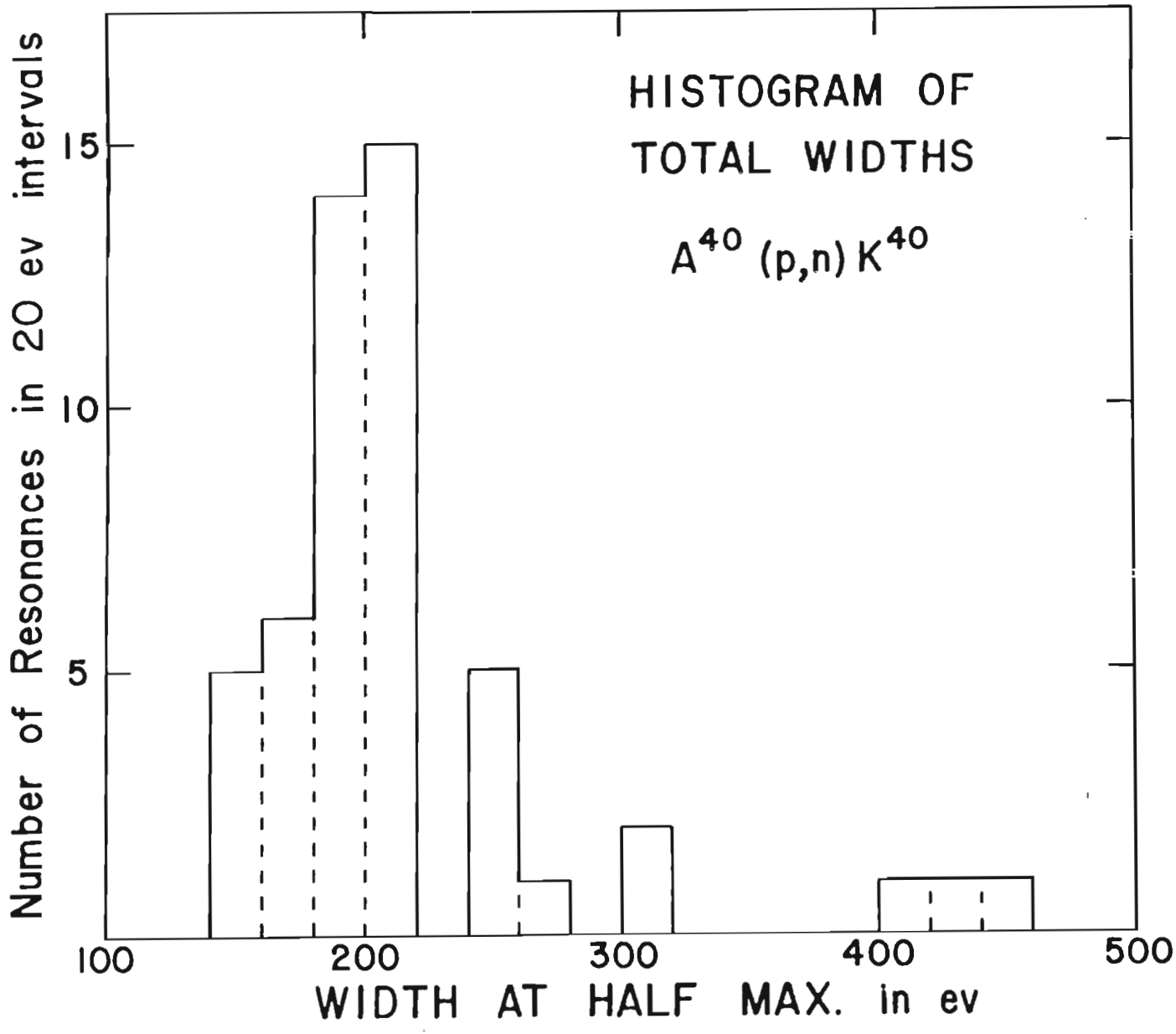
HISTOGRAM OF
TOTAL WIDTHS
$A^{40}(p,n)K^{40}$
Number of Resonances in 20 ev intervals
15
10
5
100
200
300
400
500
WIDTH AT HALF MAX. in ev

in the beam tube had been appreciable, we should have seen a smaller but wider ghost of each resonance at 2.4535 and 2.4585 Mev. However, no peak in the yield curve appears larger than expected from statistical fluctuations at either energy.

We can therefore estimate the upper limit of the argon density outside the reaction chamber relative to that inside from the statistical uncertainty of the background. Consider the resonance at 2.4615 Mev. At 3.5 kev lower energy the background (partly the tail of a preceding resonance) averages about 700 $\pm$ 26.4 counts per 10 microcoulombs. Since the energy spread of this beam (uncorrected by the homogenizer) is about 500 ev, the ghost resonance would have to be at least as wide. For the ghost to be unobservable the peak can be no higher above the average level than that allowed by statistical fluctuation alone. Thus the maximum integrated yield of this ghost can be approximated by replacing the true shape with a rectangular yield which has a height of 26.4 counts and a width of 500 ev. The integrated yield of the ghost (from summing the yield in 50 ev intervals as is done for all the real resonances) can be no greater than 264.

However, since practically all the beam pipe is outside the 4π counter, the effective solid angle subtended from the pipe by the unshielded counter is only about 0.6 steradians. Thus, if this yield were observed in a 4π detector of similar efficiency, it could amount to as much as $264 \times 4\pi/0.6 = 5700$. Comparison with the integrated yield of the real resonance at 2.4615 Mev (109,600 total counts above background) shows that the number of molecules

per cm^2 in the beam pipe relative to that in the target chamber could at most amount to about $5700/109,600 = 5.2 \times 10^{-2}$. Thus our trapping efficiency must be greater than 95%, and it is probably even better than this figure would indicate. The difference in relative lengths of the real and ghost targets (11/16" and 36" respectively) indicates the density (i.e., pressure) of the ghost target is $\leq 1 \times 10^{-3}$ the density of the real target.

The trapping efficiency should be independent of the rate at which the target gas is introduced as long as the rate is not excessive. The data in Figures 6, 7 and 8 were taken with a gas flow of 13.8 cc/min. No visible effect on the vacuum or the beam integration can be noticed until the gas flow exceeded about 40 cc/min. Thus, for argon, the gas flow can be adjusted over a wide range as long as the boiling rate of liquid helium is not too great or the neutron yield is not too small.

2. The Incident Beam Spread.

The minimum observed peak half width is a measure of the effective resolution. However, an absolute measure of the incident beam energy spread cannot yet be accomplished, since we do not know the true half width of the resonance or the effect of the proton energy lost within the target by collisions with the atomic electrons. We can obtain an upper limit for the beam spread if we choose to ascribe the entire minimum observed half width to the effect of an inhomogenous beam and Doppler effect.

Let $\phi(E_o, E_1)$ be the proton energy distribution function of a beam of nominal energy E_o before encountering the target. However, the target

atoms are not at rest. If a perfectly monoenergetic beam of energy E_1 were to encounter these nearly ideal gas atoms, the effective energy distribution function is (Bethe and Placzek, 1937)

$$g(E_1, E_2)dE_2 = 2\pi^{-1/2}\exp\left[-4(E_1-E_2)^2/\Delta^2\right] dE_2/\Delta$$

where

$$\Delta = 4(mE_1\, kT/M)^{1/2}$$

is known as the Doppler width, m = mass of bombarding particle, and M = mass of target nucleus. Thus the total energy distribution function $\Phi(E_o, E_2)$ is given by

$$\Phi(E_o, E_2) = \int_{E_1} \phi(E_o, E_1)g(E_1, E_2)dE_1$$

with the integration over the variable E_1 carried out in the vicinity of E_o.

We neglect the energy dissipation within the target and assume that the resonance at E_r has a natural width so small that we can replace the usual Breit-Wigner dispersion formula for the cross section with a delta function. The yield distribution function then becomes proportional to

$$\begin{aligned} Y(E_r, E_o)dE_o &= \int_{E_2} \Phi(E_o, E_2)dE_o\ \delta(E_r-E_2)dE_2 \\ &= \Phi(E_o, E_r)dE_o \end{aligned}$$

Thus we see that the yield distribution function is proportional to

$$(1)\quad Y(E_r, E_o) = \int_{E_1} \phi(E_o, E_1)g(E_1, E_r)dE_1$$

Suppose the initial beam energy distribution function is symmetric about the nominal energy E_o. A useful approximation for this function would be the Gaussian distribution.

$$\phi(E_o, E_1) \sim \exp\left[-4(E_o - E_1)^2/w^2\right]$$

If this form for the initial energy distribution is inserted in equation (1) we find that

$$(2) \qquad Y(E_r, E_o) \sim \exp\left[-4(E_r - E_o)^2/(\Delta^2 + w^2)\right]$$

This expression is also Gaussian and the 1/e full width is just $(\Delta^2 + w^2)^{1/2}$. However the half height full width, which corresponds to our observed half widths, is

$$(\ln 2)^{1/2}(\Delta^2 + w^2)^{1/2} = 0.83\,(\Delta^2 + w^2)^{1/2}$$

The minimum half width observed is 140 ev. Our target chamber ran at approximately 60°K and thus Δ = 70 ev. This leads to an upper limit on the half width of the incident energy distribution function of $\sim$125 ev. Investigations at Oak Ridge National Laboratory have reported that the initial beam spread as the beam leaves the ion-source is approximately 70 $\pm$ 10 ev (Moak, 1963). Until the effect of the collision process in the target is better understood, a more accurate value of beam spreads attainable with the homogenizer will be impossible.

3. The Target Thickness

In general the effective proton energy distribution at depth x in the target relative to the reaction nucleus is the integrated product of three different distribution functions, the incident beam distribution, the distribution caused in energy dissipation from prior electronic collisions, and the Doppler effect distribution caused by the thermal motion of the target atoms. When this effective proton energy distribution is multiplied by the

nuclear reaction cross section we obtain the neutron yield from the whole target, given by

$$Y(E_b, E_r) = K_1 \int_{x=0}^{T} \int_{E_o} \int_{E_1} \int_{E_2} \phi(E_b, E_o) f(E_o, E_1, x) g(E_1, E_2) \sigma(E_r, E_2) dE_o dE_1 dE_2 dx$$

where K_1 is a constant of proportionality, E_b is the nominal bombarding energy, and E_r is the resonance energy. $\phi(E_b, E_o)$ is the distribution function for the incident beam, $g(E_1, E_2)$ is the Doppler effect distribution function, and σ is the usual Breit-Wigner cross section for the (p, n) reaction characterized by the natural width at half maximum Γ. The "target profile" $f(E_o, E_1)$ is the result of integrating the inhomogeneous distribution function $f(E_o, E_1, x)$, over the entire target. When this integration is performed we have a somewhat simpler expression for the yield at bombarding energy E_b given in terms of the "target profile" by

$$Y(E_b, E_r) = K_1 \int_{E_o} \int_{E_1} \int_{E_2} \phi(E_b, E_o) f(E_o, E_1) g(E_1, E_2) \sigma(E_r, E_2) dE_o dE_1 dE_2$$

We usually approximate ϕ with a Gaussian distribution function, and, as stated before, the Doppler effect is also Gaussian. The single level Breit-Wigner expression for the nuclear cross section, σ, can also be approximated as Gaussian where the square of the 1/e width $\xi^2 = (\Gamma/0.83)^2 + (S/0.83)^2$ where Γ is the true width and S will be defined later. The form of the function $f(E_o, E_1, x)$ has been the subject of several theoretical treatments, but for various reasons the conditions of our experiment do not satisfy their basic premises. Once the principle of "straggling" (the increase of width of the effective proton distribution function with

increasing depth x) is taken into account all theories tend to predict asymmetric "target profiles", but in spite of the fact that both theory and experiment indicate an asymmetric shape, we will assume that the target profile can be considered a Gaussian to a first approximation, and discuss the finer points later.

We have thus replaced all the functions in the expression for neutron yield with equivalent Gaussians. The approximate yield function is therefore given by

$$Y(E_b, E_r) = K_2 \exp\left\{-4(E_r-E_b)^2/\left[w^2+\Delta^2+(t/0.83)^2+\xi^2\right]\right\}$$

where K_2 is a constant of proportionality, w, Δ, t/0.83, and ξ are the 1/e full widths of the various Gaussians. For our narrowest resonances, such as that at 2.4426 Mev with apparent half width = 140 ev, we assume that ξ^2 is negligible, and obtain an upper limit on the target thickness, t, by assuming the beam spread half width of 70 ev reported by Moak and Δ = 70 ev. We have

$$(70)^2 + \ln 2\,(70)^2 = t^2 = (140)^2$$

This yields a "target thickness", t = 107 ev.

We have also studied the effect on the peak shape of varying the target density. Table 2 summarizes our findings for a wider peak at 2.4615 Mev. The apparent width for the resonance in Table 2 is indeed larger than that reported in Table 1 for nearly the same flow rate but this data in Table 2 was taken during a later run. We could reproduce the integrated yields but not the widths. We believe that in the meantime, deterioration of the

Table 2. Observed Properties of 2.4615 Mev Resonance Peak with Several Target Densities

Gas Flow	Relative Integrated Yield	Apparent Half width	Ratio of Tail to Main Component	Calculated Target Thickness
7.6 cc/min	2.7	250 ev	.43	85 ev
12.4	5.0	270	.25	157
20.7	8.2	350	.27	258

source led to an increase in incident beam spread. Unfortunately the natural width does not appear to be negligible.

To analyze this data we let x be the apparent width at half maximum for an infinitely thin target, i.e., $x^2 = (w^2 + \Delta^2)\ln 2 + \Gamma^2 + S^2$. The target thickness t is directly proportional to the amount of material in the target, to the relative integrated yield, and also to the gas flow rate as shown in Table 2. We let y be the width at half maximum of the Gaussian profile for a target whose relative integrated yield is unity. Then t = ky is the thickness for any other target density where k is the corresponding relative integrated yield. Thus we have three equations and two unknowns. We calculate y from the data for the thinnest and thickest targets.

$$x^2 + (2.7\ y)^2 = 250^2$$

$$x^2 + (8.2\ y)^2 = 350^2$$

We find x = 236 ev and y = 31.4 ev. The last column shows the estimated target thickness for the various flow rates. We can check our estimate for t for 12.4 cc/min directly with the observed width and our estimate of x.

$$236^2 + t^2 = 270^2$$

or $\quad t = 131$ ev

Thus we have three reasonably consistent estimates of the target thickness --107 ev, 131 ev, and 157 ev with the gas flows approximately 13 cc/min. We prefer the lowest estimate, 107 ev, since it was obtained from the narrowest resonances where Γ should have the least effect. It should be noted in Table 2 that at the slowest gas flow, the thickness has been

reduced nearly to the value of the incident beam spread. The thinnest lithium target we can evaporate is more than five times as thick!

We can now estimate the density of our target. From interpolation of the data on average energy losses (Allison and Warshaw, 1953), a proton in argon at 2.4 Mev suffers a loss of about 81 kev cm^2/mg. Thus we must have had a target consisting of about

$$107/81 \times 10^3 = 1.32 \times 10^{-3} \text{ mg/cm}^2$$

which corresponds to 2.0×10^{16} atoms/cm^2.

Suppose the target consisted of a Van de Waals gas. Loeb (1934) shows that the Van der Waals constant b (liters/mole) is the volume "described by the hemispherical surfaces of all the spheres of exclusion of the molecules delimiting the available volume V . . ."

and $b = 4(4/3\pi r^3 N)$

where N = number of molecules/mole = Avogadro's number

Thus if the atoms of argon were arranged in layers and within each layer the atoms were separated by the distance 2r (i.e., each atom fills up area πr^2), we can obtain an estimate of the number of layers of our target. The experimental value of

$$b = .03219 \text{ liters/mole}$$

Therefore

$$r^3 = \frac{(.03219 \times 10^3 \text{ cm}^3/\text{mole})}{(16/3)(3.14)\ 6.025 \times 10^{23} \text{ atoms/mole}} = 3.19 \times 10^{-23}$$

$$\text{or } r = 3.17 \times 10^{-8} \text{ cm}$$

If each atom occupies cross sectional area πr^2 we find that the distance between nuclei can be no closer than distance 2r. Thus we can only place approximately

$$(1\ cm^2)/(4r^2\ cm^2) = 1/4.03 \times 10^{-15} = 2.48 \times 10^{14}$$

atoms in one cm^2, and therefore our target effectively consisted of

$$2 \times 10^{16}/2.48 \times 10^{14} = 81 \text{ "layers"}$$

Excitation without ionization accounts for all energy transfers less than about 15.8 ev. However, the first excited atomic state is about 11.3 ev above the ground state. Thus we can never transfer less than 11.3 ev; in effect then, practically all energy transfer leads to ionization. Bortner and Hurst (1954) find that the average energy loss per ion pair in argon is 26.4 ± 0.3 ev. But L shell ionization requires about 200 ev while the K shell ionization requires about 3.2 kev. Obviously any K or L shell ionization can contribute only to the tail of the "target profile" which lies beyond the average energy loss (the target thickness). Thus in most cases protons lost energy only through ejection of M shell electrons with an average kinetic energy of about 11 ev.

Landau (1944) and Symon (1948) have made calculations about $f(E_o, E_1, x)$ which predict asymmetric target profiles which have been used in attempts to fit the $Al^{27}(p, \gamma)$ data of Bondelid and Butler. But as these experimenters point out (Bondelid and Butler, 1963):

> "Both Landau and Symon assumed that the velocity of the incoming particle is large compared to the velocity of the electrons with which the collisions occur."

This condition is not met for either the K or L shells of argon. Furthermore they state:

> "Another limitation of both solutions, (Landau and Symon) is that neither applies to extremely thin targets because they both neglect fluctuations due to distant collisions (in which the atomic electrons cannot be treated as free)."

In Fig. 10, we see an enlargement of the prominent resonance at 2.4355 Mev which shows a marked asymmetry on the right. Every resonance in Figures 6, 7 and 8 shows this same feature. For purposes of interpretation we have broken the indicated effective distribution function into two components: (1) a symmetric "main" component(indicated by the dashed line in the figure below), and (2) an unsymmetric component or "tail" similar to the insert of Fig. 10 (indicated by the dot-dashed line).

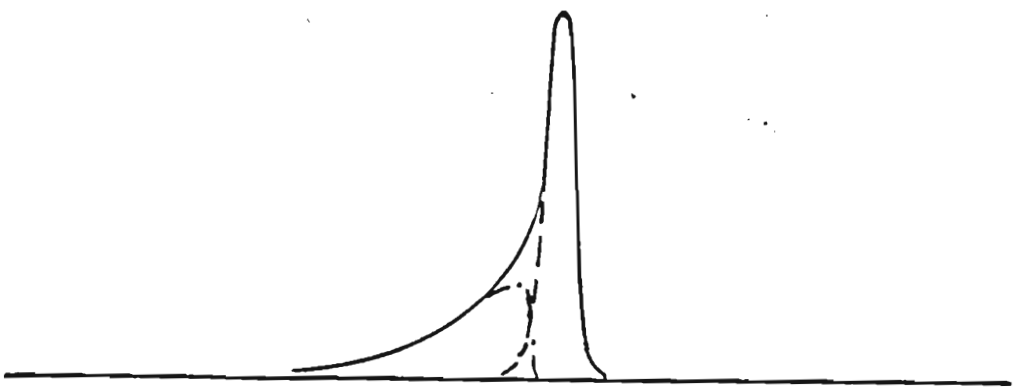

We have already considered the "main" component of the effective proton energy distribution. In Fig. 10, it will be noticed that the width at half maximum of the whole resonance is the same as that of the symmetric peak bounded on the right by the dashed line.

Figure 10. Expansion of Resonance at 2.4355 Mev to Demonstrate Assymetry of Peak.

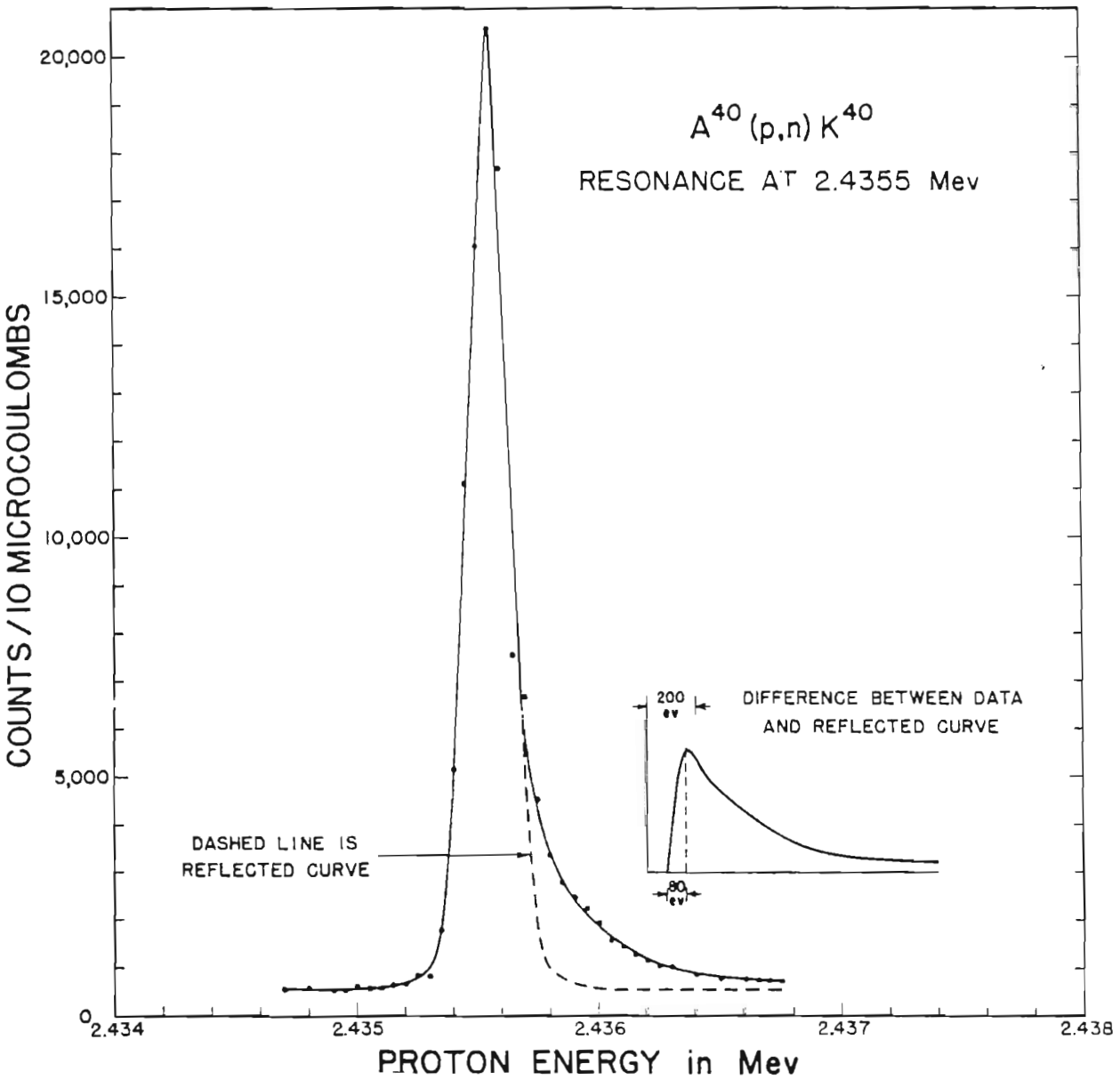
$A^{40}(p,n)K^{40}$
RESONANCE AT 2.4355 Mev
COUNTS / 10 MICROCOULOMBS
20,000
15,000
10,000
5,000
0
2.434
2.435
2.436
2.437
2.438
PROTON ENERGY in Mev
DASHED LINE IS REFLECTED CURVE
200 ev
DIFFERENCE BETWEEN DATA AND REFLECTED CURVE
80 ev

We could ascribe this observed asymmetry to the incident beam energy distribution. However, we are not equipped to study this possibility, and can only point out that none of the measurements made on the distribution of proton energies at the source have shown such an asymmetry. The processes of accelerating, deflecting, and homogenizing the protons would not be expected to introduce an asymmetry.

There are, however, arguments which indicate that the tail is due to proton energy losses, much larger than the average. All the observed reactions are the result of a proton which bores radially through the surrounding electronic cloud on a collision course to the nucleus. Thus, even for the infinitely thin target, the energy inhomogeneity which results from losses to the "reaction atom" electrons will always be present. As the target is thinned the yield distribution function should become characteristic of the contribution of the "reaction atom" alone.

There must be a real distinction between the energy loss distribution function observed in (p, n) reactions, and that for those protons which do not interact with target nuclei. For instance, the K and L electrons occupy a small fraction of the atomic volume, so that only the protons which reach the nucleus have much chance to interact with these inner electrons. Ionization of the L electrons might be one of the causes of the high energy tail of the resonance peaks in Figures 6, 7, 8, and 10. Another possibility is multiple ionization of the reacting atom before the proton reaches the nucleus. The fact that the intensity of the tail of our resonances (relative to the main

component) is practically independent of target density (see Table 2) is in accord with these explanations.

On the other hand there are as many as 31 "layers" of atoms to be traversed by each reacting proton before it reaches its target nucleus. On the average the "reaction layer" is the fortieth. Assuming that each electron-proton energy "transfer" leads to ionization, we see that the probability is only about

$$107 \text{ ev}/26.4 \text{ ev}/40 \text{ layers} = 1/10$$

for each layer. But the very large energy losses account for about 20% of the total integrated yield. If the reaction atom is solely responsible for the tail, this would lead to a probability of ionization in the reaction layer of 1/5, i.e., the probability of its ionization must be about twice the probability for prior ionizations in any of the intervening layers. If multiple ionization in the "reaction layer" is important, the ratio of probabilities must be much greater. However, such ratios are not completely out of the question because of the relatively long path which the proton follows within the "reaction atom".

If the energy losses in the reacting atoms give rise to the tail of the distributions, they must also contribute at least something to the energy spread of the main component. This contribution has been lumped with the Breit-Wigner Γ in the expression $\xi^2 = (\Gamma/0.83)^2 + (S/0.83)^2$.

We intend to pursue these investigations and try to establish the relative importance of the "last atom" within which the nuclear reaction

occurs. This is not the first time asymmetric nuclear reaction yields have been observed. Bondelid and Butler (1963) report very similar shapes for thin targets in $Al^{27}(p, \gamma)$. However, they were not certain of the effects of surface contaminants and particularly of the possible oxidation of the aluminum targets. Our measurements are, as far as we know, the first where contamination of the target cannot possibly be a complicating factor.

CHAPTER V

CONCLUSIONS

A. Cryogenic System

We have demonstrated the following properties of gases bombarded in a cryogenic system. (1) It is possible to produce a very thin and still uniform target. (2) The low temperature reduces the Doppler spread (due to molecular translation) to a negligible value. (3) Backgrounds are easily measured by removal of the target gas from the vacuum system. (4) The target length is sharply enough defined so that neutron beam experiments can be performed. (5) It is far easier to change the yield and thickness of this type of target than for a solid one. (6) Using the cryogenic target in conjunction with our homogenizer system (Parks et al., 1958) and improvements in the conventional corona control system (Kyker and Williamson, 1962), we have reduced the effective energy spread of the bombarding particle in a charged particle reaction to a much lower value than anyone has attained previously without suffering very serious slit losses. (7) In achieving this we have probably eliminated most, if not all, of the energy spread caused by potential fluctuations. (8) Further

improvements are probably possible by reducing the 70 ev source spread with an electrostatic analyzer, but a limit is set for a polyatomic molecule such as tritium by the zero point vibrations.

B. Application as a Neutron Source

Because of its low yield between resonances, the $A^{40}(p, n)K^{40}$ reaction is not generally useful as a source of monoenergetic neutrons. We do plan, however, to use the cryogenic target as the source of neutrons from the $T^3(p, n)He^3$ reaction (Newson, 1963a). In this way we eliminate the non-uniform target problem encountered with lithium. In addition a much wider energy range of homogeneous neutrons is possible with a T target since with lithium the threshold to the first excited state of Be^7 has set an upper limit at about 200 kev for our 160° neutron collimator and about 650 kev for the 20° collimator. There is no similar low lying state in He^3 to cause inhomogeneous neutron energies in the $T^3(p, n)He^3$ reaction.

When we estimate the neutron energy spread attainable with this reaction, we find that the translational motion Doppler effect and the effective proton beam spread are negligible when the 160° collimator is used. The details of the target thickness effect is still an open question but at 160° we can, in principle, make this energy spread very small simply by reducing flow rate. The two remaining causes of energy spread are the Doppler effect due to vibrational motion of each atom in the T_2 molecule and the

geometric effect due to the fact that the laboratory energy of neutron is a function of θ, the angle of the collimator. The vibrational Doppler effect has been shown (Beard, 1963) to have a Gaussian shape for its energy distribution function. However, for a detector of finite acceptance angle $\Delta\theta$, the energy distribution function for neutrons admitted should be rectangular. We follow Nichols' (1958) treatment, where the equivalent Gaussian distribution is approximated by a half width .681 times that of the rectangular function. Thus for the values of E_n, listed in Table 3, our neutron energy spread is the Gaussian sum of $\Delta E_n(\text{vib})$ and $.681\,\Delta E_n(\Delta\theta)$, i.e., $\left\{\Delta E_n(\text{vib})^2 + \left[.681\,\Delta E_n(\Delta\theta)\right]^2\right\}^{1/2}$. The estimates in Table 3 have kindly been supplied by P. M. Beard (1963).

Newson (1963b) has suggested that the tritium molecule be replaced by the H^1T^3 molecule. A mixture in which hydrogen exceeds tritium should (after catalysis) have most of the tritium in HT molecules. This scheme has the advantage that the velocity of the T^3 atom in H^1T^3 is reduced to 0.42 that of the T^3 atom in T_2^3. Thus if sufficient proton beam is available to allow us to reduce the angular spread sufficiently, $\Delta E_n(\text{vib})$ for H^1T^3 is the ultimate limit on beam spread. In Table 4 we have shown this limit as a function of E_n.

In Fig. 11 we have shown how this estimate (with $\Delta\theta = 0.3^\circ$) compares with other techniques. It will clearly be useful to develop the application of the Cryogenic Target to neutron spectroscopy. Since the nearest competitors in Fig. 11 require rather large samples (i.e., kilograms of material) our

Table 3. Predicted Beam Spread from $T_2(p,n)$ with $\Delta\theta = 0.5^\circ$

E_n	ΔE_n(vib)	$.681\ \Delta E_n(0.5^\circ)$	Neutron Energy Spread
10 kev	51 ev	55 ev	75 ev
100	112	215	242
200	131	375	400

Table 4. Predicted Beam Spread from HT(p, n) under Ideal Conditions

E_n	ΔE_n(vib)
10 kev	22 ev
100	47
200	55

Figure 11. Energy Spreads as a Function of Energy for Various Neutron Spectrometers. Solid lines represent resolutions actually demonstrated while dashed lines are estimated improvements which may be feasible. The lowest dashed line is our estimate for the HT (p, n) with $\Delta\Theta = 0.3^{\circ}$, and the dot-dash line is the latest results of the Nevis pulsed cyclotron (Havens, 1963). Portions of this graph appear in Fast Neutron Physics, Vol. II, in a chapter entitled "Neutron Cross Sections in the kev Region".

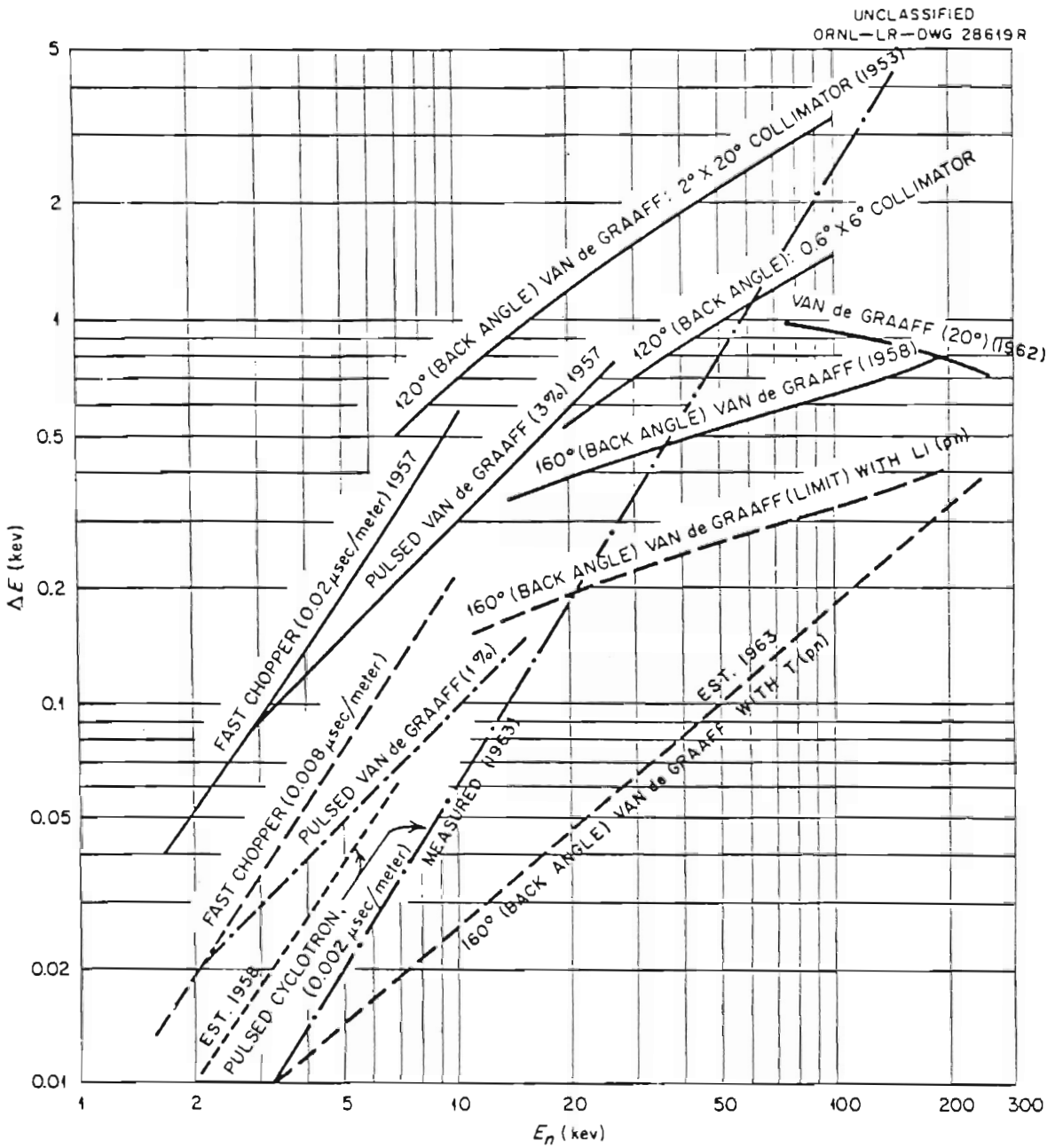
UNCLASSIFIED
ORNL—LR—DWG 28619R
120° (BACK ANGLE) VAN de GRAAFF: 2° X 20° COLLIMATOR (1953)
120° (BACK ANGLE): 0.6° X 6° COLLIMATOR
VAN de GRAAFF (20°) (1962)
160° (BACK ANGLE) VAN de GRAAFF (1958)
PULSED VAN de GRAAFF (3%) 1957
FAST CHOPPER (0.02 μsec/meter) 1957
160° (BACK ANGLE) VAN de GRAAFF (LIMIT) WITH LI (pn)
EST. 1963
160° (BACK ANGLE) VAN de GRAAFF WITH T (pn)
MEASURED (1963)
PULSED VAN de GRAAFF (1%)
FAST CHOPPER (0.008 μsec/meter)
EST. 1958
PULSED CYCLOTRON, (0.002 μsec/meter)
ΔE (kev)
E_n (kev)
5
2
1
0.5
0.2
0.1
0.05
0.02
0.01
1
2
5
10
20
50
100
200
300

target will be developed for use with 10 - 100 g samples which are available as separated isotopes.

At present only the Li(p, n) and T(p, n) reactions appear to be suitable for neutron spectroscopy below 1 Mev, but higher proton energies than we now have, or improved methods of reducing backgrounds with d, n reactions, may possibly develop other such uses of the cryogenic target.

C. Other Applications

Charged particle experiments are usually easier to perform than neutron studies because of their less intense beams. We are at present attempting the same sort of interpretation on our $A^{40}(p, n)K^{40}$ resonances that is used in neutron scattering experiments (Bowman et al., 1962). However, we still lack a measurement of the density of the target gas and of the absolute cross section. In principle this can be done by comparing integrated yields of our results with the integrated yield from a simple gas cell, where it is easy to measure the number of target nuclei per cm^2. We should then be able to analyze the data for level spins and parities, particle widths, and level spacing. To aid in this procedure we have already measured the relative differential cross sections at 0^o and 90^o.

In addition to A^{40} we have made preliminary measurements on B^{11} (in BF_3), C^{18}, and Cl^{37} (in Freon 12), and demonstrated the feasibility of obtaining sufficient yield to study each reaction. Many more gases would make useful targets if the cryostat were used with a tandem accelerator.

All this serves to show that the cryogenic target can be a rather versatile instrument where the highest resolution is required. We feel that any increased experimental difficulty associated with its use is more than compensated by the net gain in resolving power.

LIST OF REFERENCES

LIST OF REFERENCES

S. K. Allison and S. D. Warshaw, Rev. Mod. Phys. 25, 779 (1953).

P. M. Beard, oral communication (1962).

P. M. Beard and G. C. Kyker, Jr., unpublished "Duke University Nuclear Structure Laboratory Report to the Nuclear Cross Section Advisory Group" (October, 1962).

P. M. Beard, written communication (1963).

H. A. Bethe and G. Placzek, Phys. Rev. 51, 450 (1937).

R. O. Bondelid and J. W. Butler, written communication (1963).

T. E. Bortner and G. S. Hurst, Phys. Rev. 93, 1236 (1954).

C. D. Bowman, E. G. Bilpuch, and H. W. Newson, Annals of Physics, 17, 319 (1962).

J. R. Clement and E. H. Quinnell, Rev. Sci. Instr., 23, 213 (1952).

L. Davis, D. E. Nagle, and J. R. Zacharias, Phys. Rev. 76, 1068 (1949).

A. J. Dessler, "The Amplitude Dependence of the Velocity of Second Sound," unpublished Ph.D. dissertation, Duke University (1955).

A. O. Hansen and J. L. McKibben, Phys. Rev. 72, 703 (1947).

W. W. Havens, "Proceedings of the International Conference on Fast Neutron Physics," Houston, Texas, to be published (1963).

R. G. Herb, oral communication (1961).

G. C. Kyker, Jr. and R. M. Williamson, Rev. Sci. Instr. 33, 872 (1962).

L. Landau, J. Phys. (U.S.S.R.) 8, 201 (1944).

L. B. Loeb, The Kinetic Theory of Cases (McGraw-Hill, New York and London, 1934) 301-306.

C. D. Moak, oral communication (1963).

H. W. Newson and R. H. Rohrer, Phys. Rev. 94, 654 (1954).

H. W. Newson, R. M. Williamson, K. W. Jones, J. H. Gibbons, and H. Marshak, Phys. Rev. 108, 1294 (1957).

H. W. Newson and W. M. Fairbank, oral communication (1958).

H. W. Newson, "Proceedings of the International Conference on Fast Neutron Physics," Houston, Texas, to be published (1963) (a).

H. W. Newson, oral communication (1963) (b).

H. W. Newson and J. H. Gibbons, "Neutron Total Cross Sections in the kev Region," Fast Neutron Physics (to be published) (1963).

P. F. Nichols, E. G. Bilpuch, and H. W. Newson, Annals of Physics 8, 250 (1959).

P. B. Parks, R. M. Williamson, and H. W. Newson, Rev. Sci. Instr. 29, 834 (1958).

K. R. Symon, "Fluctuations in Energy Lost by High Energy Charged Particles in Passing through Matter," unpublished Ph.D. dissertation, Harvard University (1948).

R. E. Warren, J. L. Powell, and R. G. Herb, Rev. Sci. Instr. 18, 559 (1947).

R. M. Williamson, oral communication (1962).

BIOGRAPHY

Paul Blair Parks III

Born: November 20, 1934, Erwin, North Carolina

Education:

B.S.	Duke University	1957

Professional Societies:

American Physical Society
Sigma Xi

Positions:

Research Assistant	Duke University	1957-present

Publications:

Method of Canceling Energy Fluctuations of a Van de Graaff Ion Beam (with Newson and Williamson) Rev. Sci. Instr. 29, 834-839 (1958).

Abstracts:

A Windowless Gas Target Chamber Using Cryogenic Techniques (with Beard, Bilpuch, and Newson) Bull. Am. Phys. Soc. 8, 48 (1963).

High Resolution Measurement of the $A^{40}(p,n)K^{40}$ Relative Cross Section (with Beard, Bilpuch, Farrell, Kyker, and Newson) Bull. Am. Phys. Soc. 8, 48 (1963).